UCRL-CR-121818
S/C - B234561

Experimental Study of ELF Signatures Developed by Ballistic Missile Launch

S. G. Peglow
T. M. Rynne

April 8, 1993

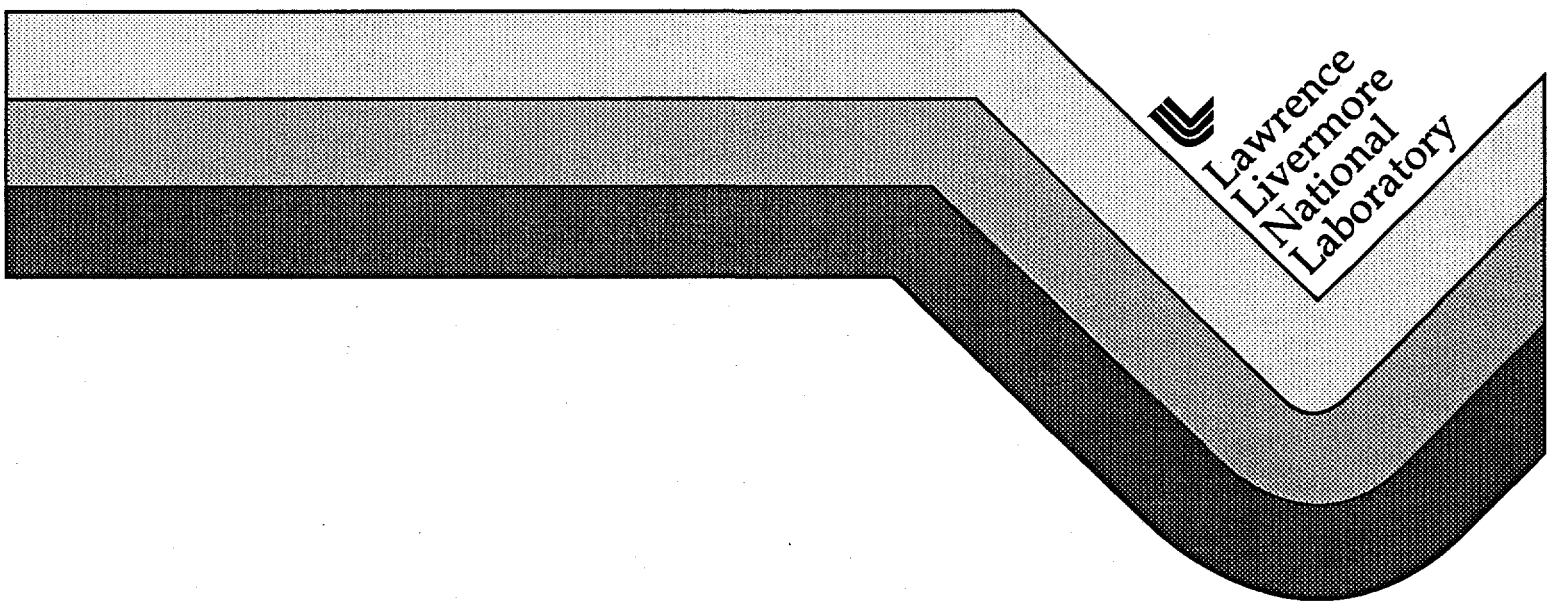

Work performed under the auspices of the U.S. Department of Energy by Lawrence Livermore National Laboratory under Contract W-7405-Eng-48.

Experimental Study of ELF Signatures Developed by Ballistic Missile Launch

Steven G. Peglow, LLNL
Timothy M. Rynne, Science Applications and Research Associates, Inc.

April 8, 1993

Prepared Under
Lawrence Livermore National Laboratory
Subcontract Number B234561

Table of Contents

List of Figures

1.0 Introduction

The Lawrence Livermore National Laboratory (Livermore, CA) and SARA, Inc. participated in the ATMD missile launch activities that occurred at WSMR during January 1993. These tests involved the launch of Lance missiles with a subsequent direction of F-15Es into the launch area for subsequent detection and simulated destruction of redeployed missile launchers. LLNL and SARA deployed SARA's ELF sensors and various data acquisition systems for monitoring of basic phenomena. On 25 January 1993, a single missile launch allowed initial measurements of the phenomena and an assessment of appropriate sensor sensitivity settings as well as the appropriateness of the sensor deployment sites (e.g., with respect to man-made ELF sources such as power distributions and communication lines). On 27 January 1993, a measurement of a double launch of Lance missiles was performed. This technical report covers the results of the analysis of latter measurements.

An attempt was made to measure low frequency electromagnetic signatures that may be produced during a missile launch. Hypothetical signature production mechanisms include

1) Perturbations of the earth geo-potential during the launch of the missile. This signature may arise from the interaction of the ambient electric field with the conducting body of the missile as well as the partially ionized exhaust plume.

2) Production of spatial charge sources from triboelectric - like mechanisms. Such effects may occur during the initial interaction of the missile plume with the ground material and lead to an initial "spike" output. Additionally, there may exist charge transfer mechanisms produced during the exhausting of the burnt fuel/oxidizer. This second type of mechanism may lead to a net dipole moment that may be significantly greater than the simple earth geo-potential induced electric field perturbation.

3) Production of signatures that are indicative of charge transfer effects in turbulent eddy zone of the exhaust plume. While the signature discussed in Item 1 above would have a relatively slow temporal behavior, this third mechanism might appear as high frequency components indicative of the turbulent effects.

A set of voltage-probe antennas were used to monitor the local electric field strength induced by geo-potential physics as well as modifications induced by the launch at ranges of approximately 1 kilometer.

Simple examination of the data acquired during the launch period failed to show a simple fiducial structure of field variations with the launch event. More sophisticated post processing was required to identify event dependent data. Several reasons can be ascribed to this initial lack of event data:

1) The sensors were not optimized for detection of the signatures induced by the missile launch. The sensors used for these measurements were originally designed for use in a personnel motion detection study conducted by SARA, Inc. for DARPA under its SBIR program. One of the sensors (designated ELF0) had a low pass cutoff frequency on the order of 100 Hz, a high pass cutoff frequency on the order of 3 Hz as well as notch filters for reducing the signature induced by the local power grid. The other sensors were prepared for the WSMR tests and had extended band ranges for detecting a wider range of signatures. These sensors (designated MLD 1, 2, 3, and 4 had internal cutoff frequencies of 2 kHz and 0.2 Hz, respectively. However, post test examination of the antennas on these second type of sensors showed that the potting antenna base potting compound had a conductivity which increased the high pass cutoff frequency from 0.2 Hz to the several Hz regime. The relatively high frequency of the high pass cutoffs would basically eliminate the ability to detect the slow temporal variation induced by the interaction of the missile/plume with the earth geo-potential.

2) The electric field potential variations have a limited spatial correlation length - the fields measured in one region have little correlation to measurements made at distances of a kilometer away. The potential variations are related to localized atmospheric disturbances and are generally unpredictable. A value for the spatial correlation length is also not known.

3) The conductivity of the plume and missile body are not adequate to produce a field perturbation of adequate magnitude. However, phenomena related to the exhaust plume and missile may exist and be outside of the collection range of the equipment employed for these measurements as described in Item 1 above.

4) The presence of 60 Hz power line noise was of sufficient magnitude to irreversibly contaminate measurements. This was particularly true for data obtained with sensors at the site at the end of Road 237. A power distribution line was quite near to this site and no notch filters were available for these sensors.

5) The presence of fairly significant background noise probably induced by lightning physics in earth-ionosphere cavity. This leads to a large number of "impulse-like" signatures that make identification of a simple fiducial associated with the launch quite difficult.

6) Time - tieing of the waveforms between the various detection sites was not handled in a very precise manner. This lead to time offsets in the waveforms (established by performing a cross correlation analysis) that was on the order of several seconds.

However, post processing of the data showed that a few of these difficulties could

be eliminated. Cross-correlation techniques allowed for the determination of the appropriate time shift needed to synchronize the data and directly compare measured signals between the various sites. Additionally, spectral analysis of the data showed that the primary noise effects were associated with signals propagating in the earth-ionosphere cavity. This was indicated by numerous resonances starting at 7 to 8 Hz and progressing upward in steps of about 7 Hz. Numerical decimation of the data to below 10 Hz resulted in a waveform for the ELF0 detector that readily shows a transient that occurred at the time of launch and which does not show extensive pulse-like contamination over the measurement window.

2.0 Scientific Premise

The simplest signal production mechanism that can be envisioned involves the perturbation induced by the missile and its plume interacting with the geo-potential field. The geo-potential field above the earth's surface is caused by cosmic ray and natural radiation leading to an ionization of the atmosphere as well as a small net current density. This in conjunction with additional currents induced by the distribution of thundercells around the planet leads to an electric field distribution in the earth-ionosphere cavity. The electric field gradient near the ground and at sea level is approximately 150 V/m for fair weather conditions and exhibits variations due to local weather and diurnal effects. A conducting object placed within this field will locally alter the field distribution.

The primary premise for this experiment was that the presence of the missile body and exhaust plume conductivity would provide a perturbation that could be detected. Detection of this slow variation in field would depend on spatial correlation and magnitude of naturally occurring variations in the ambient field as contrasted against this slowly varying temporal field. SARA, Inc. measurements for personnel detection schemes had already shown that detection of fields down to one thousandth of ambient could be used for successful discrimination of personnel over ambient signatures. As part of the WSMR measurements, it would be necessary to characterize the ambient noise characteristics in temporal/frequency domains of interest to missile launch detection.

In Section 2.1 we provide a simple theoretical estimate for the temporal variation of the plume conductivity. This result along with simple transmission line propagation analysis implies that the missile plume provides a fairly long conductor which effectively shorts out the ambient geo-potential induced electric field. Accordingly, in Section 2.2 we provide a theoretical estimate for the field perturbation that would be produced by a missile that has a fixed vertical acceleration. The temporal variation can be contrasted against the bandwidth characteristics of the detection system in order to assess whether or not the present baseline instrumentation would be appropriate for measuring the predicted field perturbation.

Besides this simple physical mechanism, other processes may lead to signatures in the low frequency band. These include phenomena that relate to triboelectric effects (arising from interaction of the missile plume with either the ground or the missile/thruster structure) as well as turbulent eddy effects that lead to higher frequency excitations than those predicted by the simple quasistatic model for the interaction of the ambient geo-potential field with the missile/plume system. We have not developed a theoretical model of these signatures but have kept them in mind in examining the data for possible signatures that may be of use in detecting a missile launch.

2.1 Estimate for Plume Conductivity Versus Time

SARA, Inc. developed a simple model for estimating the conductivity of the plume material as a function of time after exhausting from the missile. This analysis assumes that the initial material is highly ionized after combustion and through electron attachment, electron-ion recombination, and ion-ion recombination eventually returns to ambient conductivity. For this analysis, nominal values for the various three parameter air chemistry parameters (i.e., electron plus single species positive and negative ions) were assumed in calculating carrier species densities as a function of time. Similarly, nominal mobility values for electron and fast ions were assumed in determining the total conductivity of carriers.

Figure 2.1-1 shows the resulting conductivity versus time profile provided by this analysis. The model does not include all of the complexities of exhaust expansion effects on the air chemistry, effects of turbulent mixing as well as evolution of the ion species to slow ions; however, the resulting curves do show that the plume takes a long time to return back to ambient conductivity values. Also note that while we assumed that the ionization fraction was very high for these specific results, parametric and asymptotic analyses show that the late time behavior is very insensitive to initial assumptions (i.e., the plume quickly loses memory of initial conditions).

Based on these results, we performed some additional analysis of the characteristic propagation length for signals along the plume based on a simple transmission line analysis. This analysis showed that the effective plume length in the few Hz regime would be on the order of a kilometer. Thus, we developed a model of the interaction of the ambient geo-potential induced electric field with the missile plume system based on a simple assumption that the plume appeared as a highly conducting channel (in comparison to the ambient air conductivity) and lead to an effective shorting of the electric field in the plume volume.

2.2 Nominal Estimate for Geo-potential Perturbation

The estimate for the field perturbation versus range from the launch location was based on a simple prolate spheroid geometry. The launch was assumed to be vertical in direction and a constant velocity of Mach 3 was assumed for the missile. In an attempt to crudely account for the physical expansion of the plume, the plume diameter at the ground level was assumed to be 3 meters over the duration of the launch. Additionally, for the sake of simplicity, the plume conductivity was assumed to be to be much higher than ambient and be constant throughout the plume volume and throughout time.

Figure 2.2-1 shows the resulting estimate for the resulting electric field perturbation versus time seen by a ground observer at various ranges. The ambient geo-potential induced field was assumed to be 150 V/m. Note that the time to peak for these curves is somewhat dependent on range with peaks occurring in the hundreds of seconds

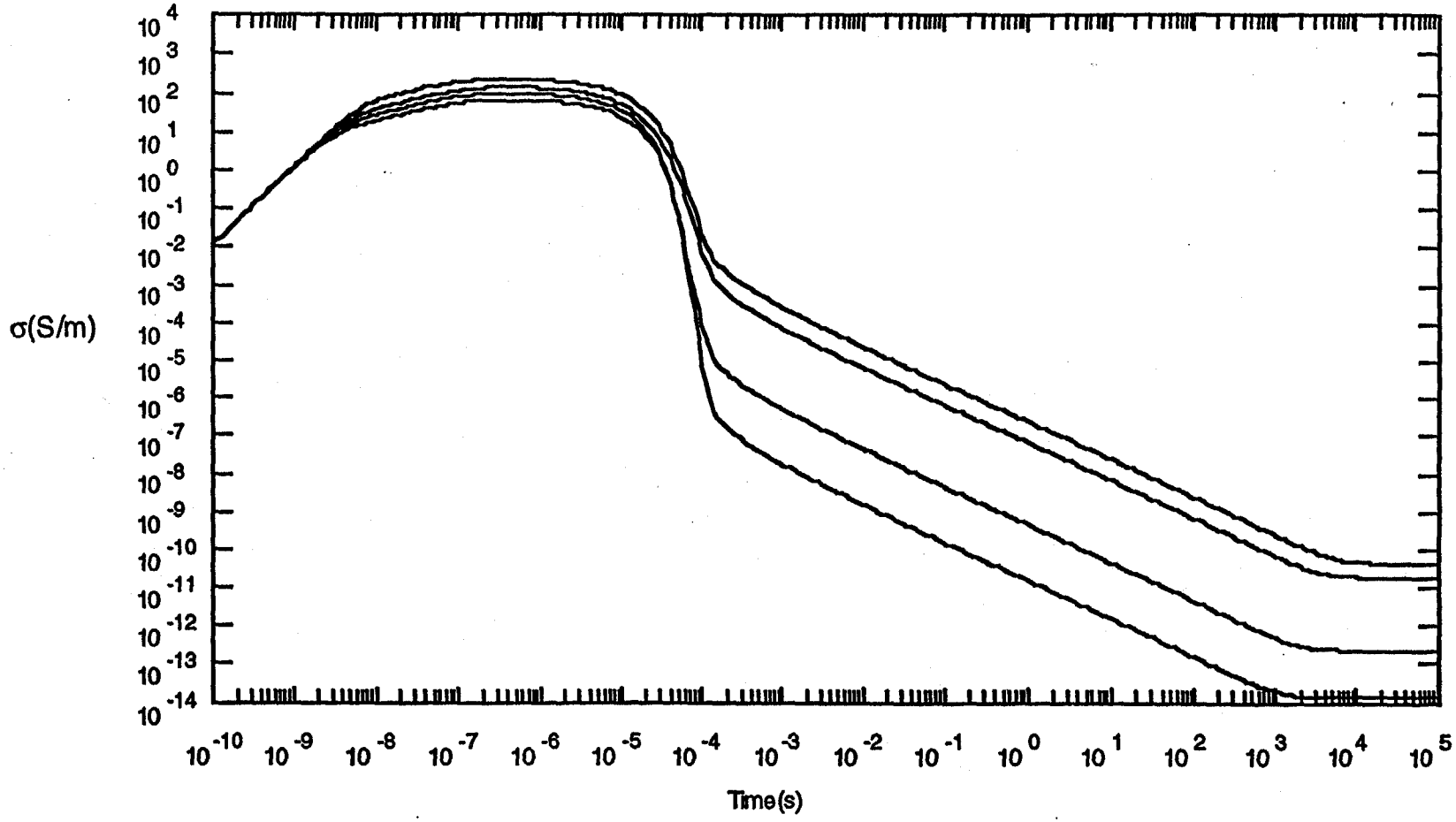

Figure 2.1-1: Estimate for Plume Conductivity Versus Time Since Exhaust for Various Initial Temperatures. Note that ambient conductivity values (late time flat plateau) are not reached until well into the multisecond time regime. Plume temperatures vary from 300 °K (lowest curve) 30,000 °K (upper curve) in uniform logarithmic steps. For a Mach 3 vehicle, these results implies fairly long time regimes before the plume conductivity returns to ambient levels.

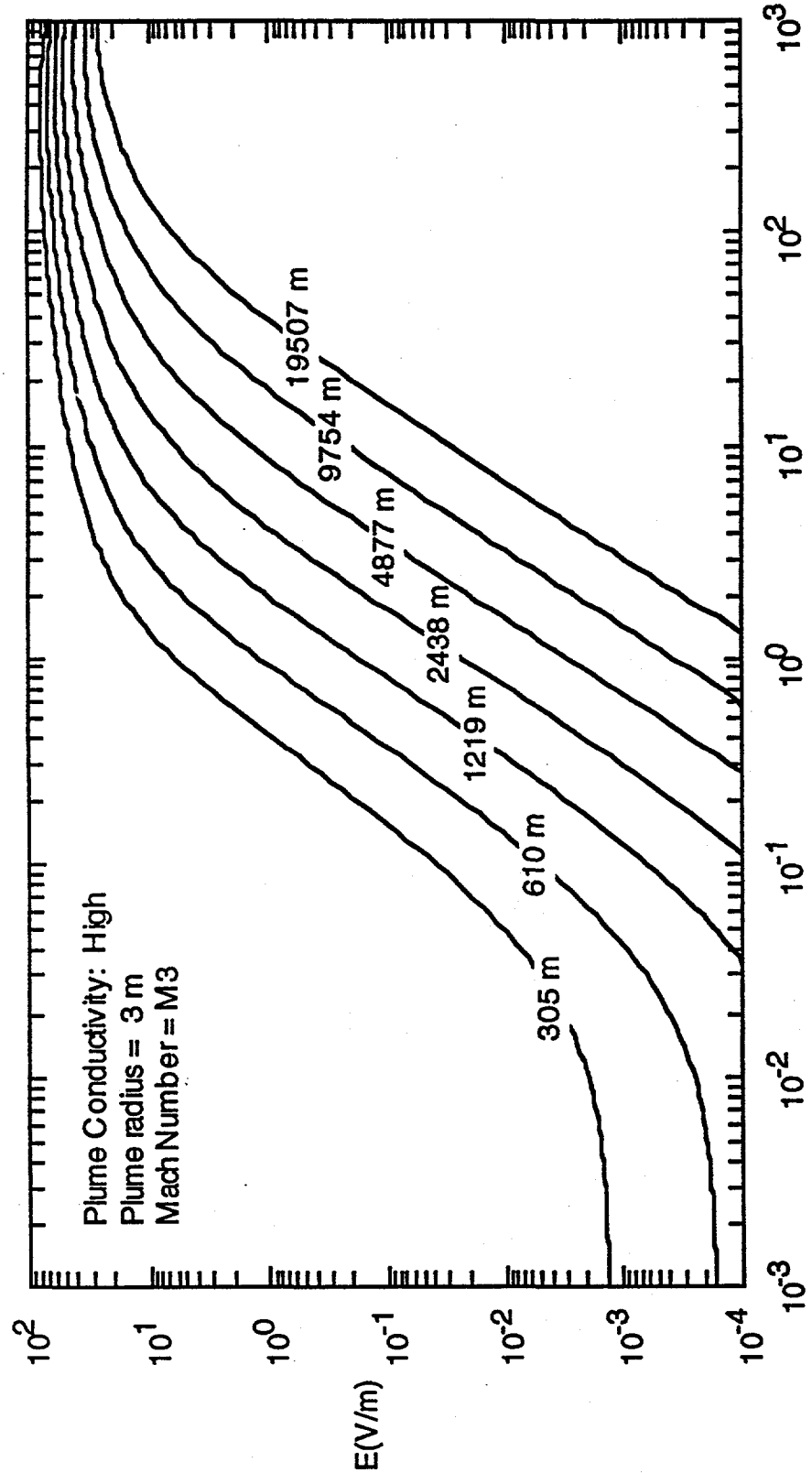

Figure 2.2-1: Estimate for Field Perturbation Versus Time For Various Ranges from Launch Location. Plume Conductivity was assumed to be much higher than the ambient air conductivity.

regime. We must note that air chemistry effects will tend to heavily erode the increased conductivity by this time and therefore we expect that the actual waveform will likely peak in the seconds to tens of seconds regime. These results imply that an optimal detector for observing this phenomenon should have a excellent response down to at least 0.1 Hz. Additionally, from these results and the realization that the actual peaks will be moved back to earlier times, we find that the peak field perturbation for a ground observer at the 1 kilometer ranges should be on the order of 10 volts.

3.0 Measurement System

Two types of measurement systems were used for the ATMD tests. The first type of system (designated ELF0) was previously developed by SARA, Inc. in 1991 under private internal funds. This detector and associated electronics is described in detail in Section 3.1. Additionally, a second set of sensors were fabricated under SARA, Inc. internal private funds specifically for use in the ATMD tests. These detectors had extended bandwidths beyond the original ELF0 device. This redesign was intentionally effected in an attempt to monitor a broader range of phenomena than could be monitored by the bandwidth restricted ELF0 device. A basic description of this device is supplied in Section 3.2.

3.1 ELF0 Probe System

Figure 3.1-1 provides a layout of the sensor/preamplifier system that SARA, Inc. (originally developed under an internal SARA, Inc. activity) to measure near-field electric fields developed in the Sub VLF regime. The following is a description of the baseline design of the sensor and preamplifier unit.

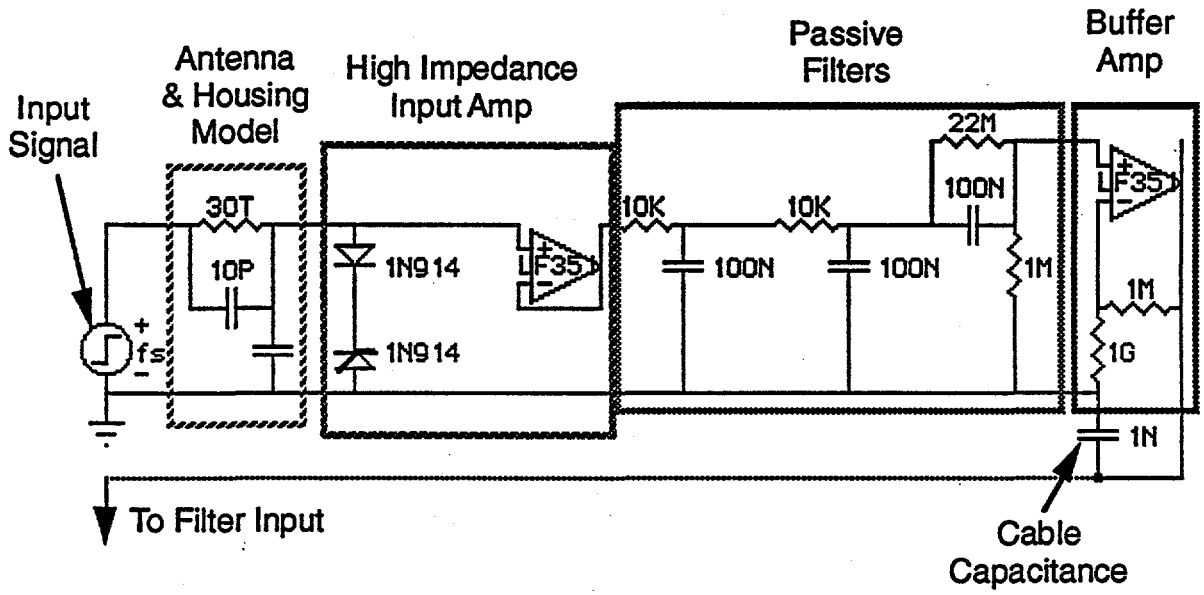

Figure 3.1-1: Electrical Layout of Sensor/PreAmp Assembly. Output from this device is sent to a set of filters and subsequently to the Data Acquisition System and Controller. (Note on Indices: P is pico, N, is nano units. Note on Units: Resistances in Ohms, Capacitances in Farads.)

The design is fairly straightforward once an understanding of the field production mechanisms and the atmospheric electrical properties are combined with the input preamplifier design. The output from the electric field sensor (antenna) is tied to the

input of a JFET input operational amplifier. Figure 3.1-1 provides analytic estimates for the input capacitance and resistance of the antenna to a far field source as well as the parasitic capacitance of the antenna/preamplifier enclosure back to local ground. The high impedance ($10^{12}\ \Omega$) of the amplifier leads to a flat, approximately unity gain frequency response above a frequency which is proportional to the inverse of the antenna capacitance to near ground and the input impedance of the amplifier. Note that the preamplifier requires a small bias current (pA regime) in order to avoid drift and saturation effects. For this reason as well as to provide electrical protection, two back-to-back 1N-914 diodes were placed at the front end of the LF 353. Note that the LF 351 model inherent in the electrical modeling code library that was used for numerical simulations was used to represent half of an LF 353 (there are two independent operational amplifiers on each LF 353 chip). This drops the preamplifier input impedance down to about $10^9\ \Omega$. For the antenna size used in our prototype system the breakpoint frequency is on the order of 10 Hz.

The increased capacitive impedance at lower frequencies leads to a fall-off in the signal response of the preamplifier that is proportional to frequency. At very low frequencies (below roughly the inverse of the dielectric relaxation time of the atmosphere or about 3 mHz), the resistive loading of the antenna through the conductive air channel will dominate and the response flattens out to a gain value given by the ratio of the preamplifier input impedance to that of the input resistance from the air to the antenna (see Figure 3.1-3 for the frequency domain transfer function of the full preamplifier/filter assembly). Such a behavior has the advantage of rejecting the relatively large "DC" component of the ambient atmospheric field while not greatly reducing signals in the several Hz and higher regime.

Finally, the preamplifier has an additional amplifier stage to ensure sufficient signal strength such that cable leakage between the preamplifier and the filter box does not significantly degrade, and to match the output line impedance. The 1 GΩ resistor indicated in Figure 3.1-1 can be set to other discrete values allowing for a net gain of X1, X10, and X100. This allows for a boost in the output signal so that leakage in the cable run (RG-59 coaxial cable over a distance of about 10 m) between the sensor and the Data Acquisition system does not become significant.

Figure 3.1-2 provides a circuit layout of the filter assembly that was used in our test activities. This filter assembly was used to eliminate low frequency noise outside the range of interest for detecting personnel motion, remove strong power distribution induced signals (allowing for larger dynamic range for signals of interest) and to remove the possibility of frequency aliasing in the digitization process.

Active notch filters are included to reduce the 60 and 180 Hz signals produced by local power distribution systems. Without notching, the 60 and 180 Hz signals would push the peak-to-peak level of the time domain signal and thereby impose severe quantized limitations on the digitally converted signal. Both notch filters are based on active filters driven by a twin T filter, with an additional op amp included in a feedback

loop so that the Qs of each filter can be adjusted. Since the components of the twin T are not exactly matched (2% components were used) adjustment of the Q is used to maximize rejection of a given frequency component.

Besides notch filters, we have also incorporated multipole high and low pass filters. The high pass filters are used to cancel out 1/f "popcorn" signals that are generated in the preamplifier, as well as DC offset signals that are produce by imbalances in the amplifiers and battery power source. The low pass filters are used to suppress high frequency signals (VLF and above) that would lead to aliasing in digitally sampling the signals. The output of the filter box is again actively amplified and matched to the signal line. As shown in Figure 3.1-2, the output cable capacitance, and DAS

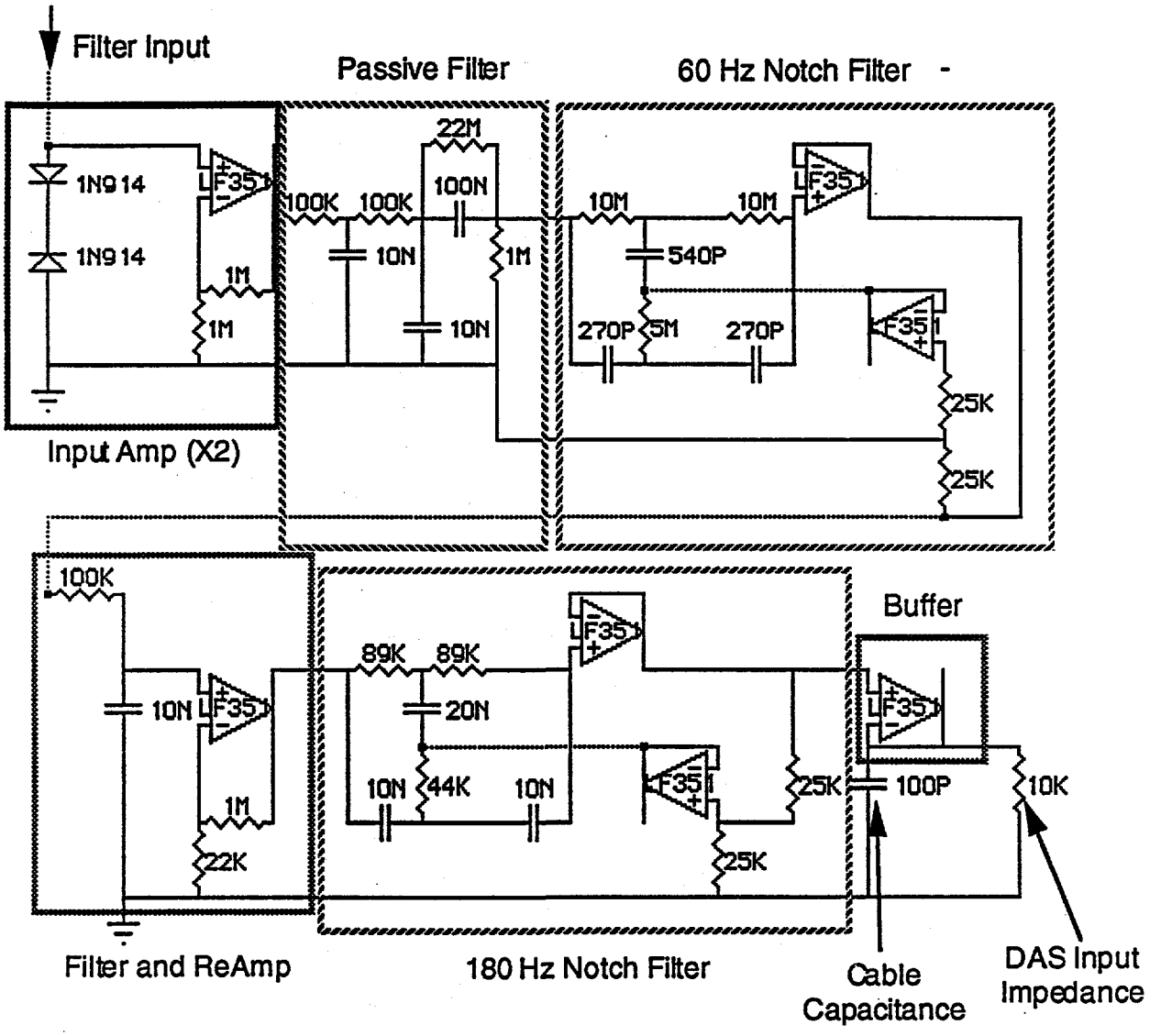

Figure 3.1-2: Electrical Layout of Filter Assembly. Input comes from the sensor/preamplifier assembly.

termination impedance has also been incorporated into the circuit model for estimating system response.

The analog-to-digital conversion box is a commercially available MACADIOS 8ain Data Acquisition System (DAS). We have modified the MACADIOS unit to take direct DC power instead of the original AC power required by the device. This unit has 8 channels and a maximum sampling rate of about 30,000 samples per second with a 12 bit resolution. This DAS has a sampling rate which is sufficient for measuring any S-VLF signals without causing undue aliasing. The DAS has a variable input gain that can be set to values of X1, X10, X100, X200, and X500.

The DAS is presently controlled by a Macintosh PowerBook 170 computer. This computer stores and post processes the data for identification of signal attributes that may be exploited for "target" identification. Besides the elements shown in Figure 3-1. the full signal acquisition system has been placed in a metal attache case with internal DC 12V battery power to eliminate grounding and noise effects from any AC power source.

Besides the physical features of the analog electronics, we also select digitizing rates such that the Nyquist half-band frequency "folds" any higher harmonics of the 60 Hz power signals back onto the lower 60 Hz harmonics. This folding concentrates any aliased power signals into easily identifiable spectral lines for post-processing and removal.

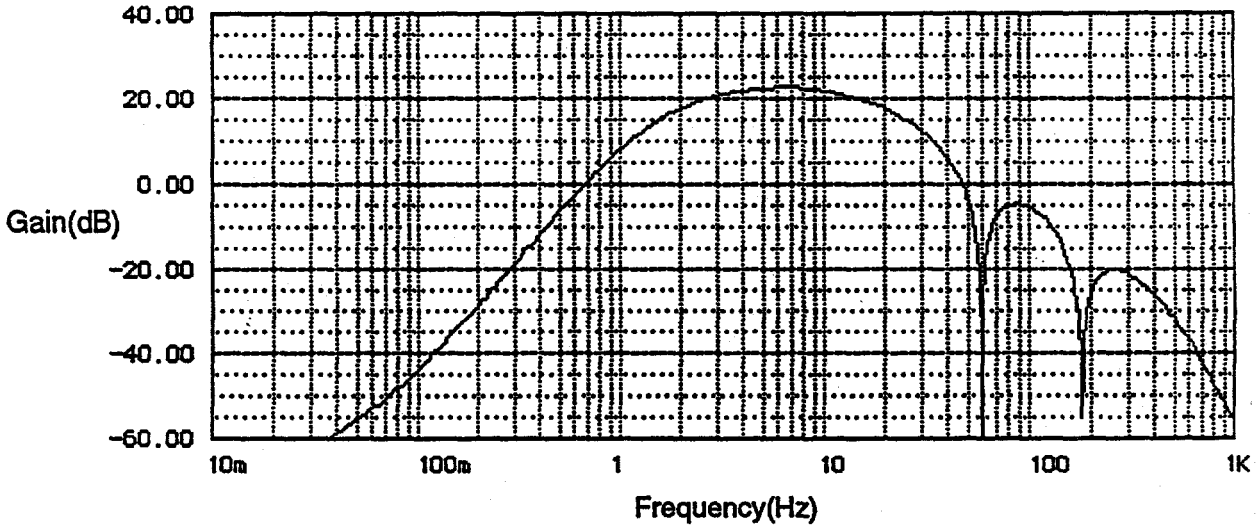

Figure 3.1-3: Calculated Frequency Response of Monopole ELF0 Sensor with PreAmp and Filter Assembly Run into DAS.

3.2 Modified S-VLF Detectors

In order to look for wide bandwidth signature, we fabricated four detectors that had a low pass filter structure that would allow measurement to higher frequencies. Additionally, the high pass structure was modified to produce a smaller roll off in the sub Hertz regime. Figure 3.2-1 shows the predicted frequency response for these sensors. The sensors have an output buffer amplifier that can be adjusted from unity gain up to X10,000. The result shown in Figure 3.2-1 is for the specific case of unity gain in the output amplifier.

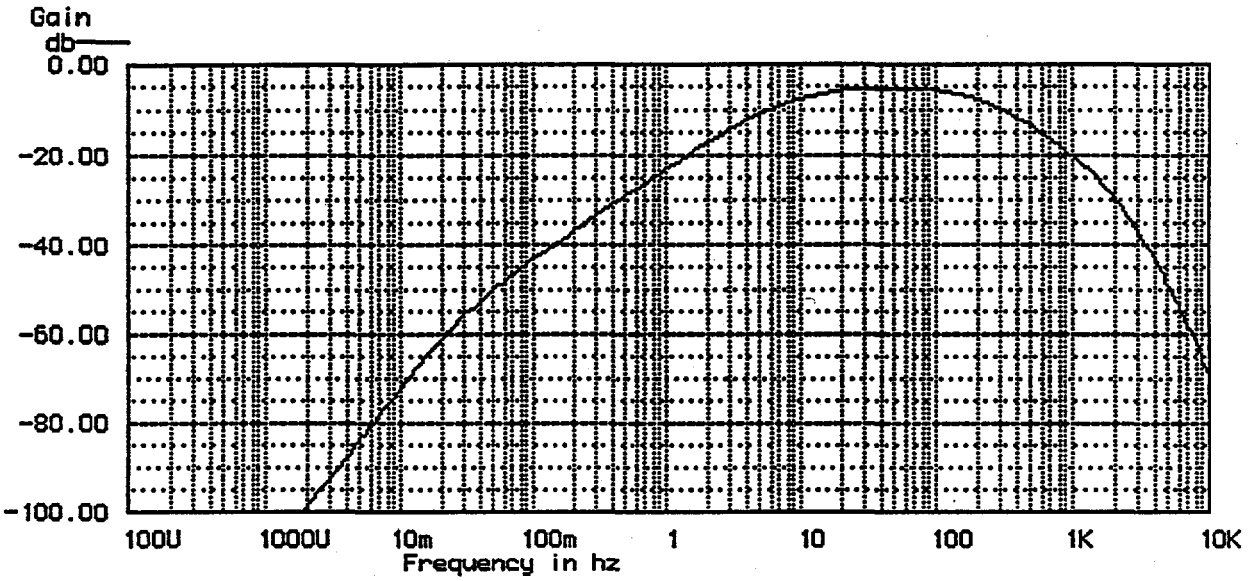

Figure 3.2-1: Response of Increased Bandwidth (MLD) Detectors.

These detectors were set up in pairs in a gradiometer configuration with a baseline separation of about 12 m between the vertical monopole antennas. Each antenna had a net vertical height of about 2.5 m. The output from these detectors were run to a Sony Digital Acquisition Tape (DAT) recorder. A single gradiometer configuration was deployed at both the 473 benchmark site as well as the site at the end of Road 237.

For final transfer to computer, the DAT was fed back into the MACADIOS DAS and the tapes were sampled over short windows of about 35 seconds duration around the time of launch of the two missiles. The tapes were sampled at a rate of 555.532 μs per sample. This sample rate would ensure that any aliasing of 60 Hz harmonics would map back onto lower 60 Hz harmonic components. The record length was restricted by the 65536 sample length restriction of the MACADIOS DAS.

3.3 ATMD Measurements

The measurement hardware (probes and recorders) were placed at different locations during the launch events on 1/25/93 and 1/27/93. During the first launch event all sensors were placed at Chat site in a distributed array. The locations indicated as 473 and 237 as well as Chat were used for the later launch events. Figure 3.3-1 shows the locations of these measurement locations as well as the location of the launch site.

At the 237 and 473 sites, the gradiometer configurations were aligned radially from the launch site. The DATs at these sites were started at about 15 minutes prior to scheduled launch time. Subsequently, the tapes were recorded into a PowerBook 170 through the MACADIOS DAS for analysis. The record was roughly centered about the actual time of launch.

Note that time-tieing between the DAT recorded sensors was fairly crudely performed by synchronization by a simple watch. At the Chat site, the time-tieing was even cruder owing to the need to deploy the ELF0 sensor further away from the power line at Chat. This resulted in the need to have the countdown shouted to the DAS operator over a distance of a couple hundred meters. This plus reflex delays and actual launch time delays lead to significant uncertainty in synchronization of the various data records.

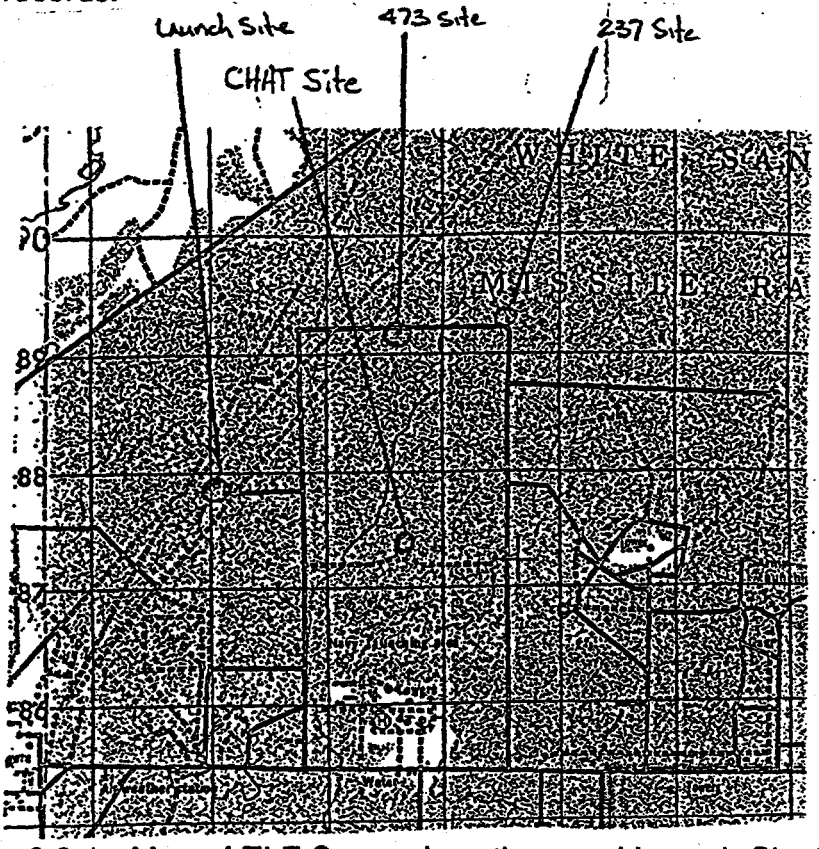

Figure 3.3-1: Map of ELF Sensor Locations and Launch Site Location.

4.0 Data Analysis

The data collected during the launches was examined off line. A significant amount of power line noise was present in the data. The 60 Hz power lines in the region resulted in contamination of all recordings with related noise. The acquisition equipment was battery powered and therefore did not contribute to the source of the noise.

4.1 Simple Time Domain Signal Comparison

Initially, a simple analysis was performed in an attempt to identify any signatures that may be produced by the missile launch. Figure 4.1-1 shows the resulting comparison of the data obtained at the three deployment sites centered around the first launch conducted on 1/26/93. The raw data was smoothed by a simple moving average in order to kick out the 60 Hz component. However, significant "noise" is still left in the data. While suspect peaks are indicated (???), such discrimination is questionable. Numerous peaks present themselves as candidates for consideration. Additionally, the peaks are offset by considerable times even though we attempted to synchronize by hand as closely as possible.

In order to determine if the identified peaks are appropriate candidates, we have performed additional analyses to optimize time tieing between the data and to determine if the noise induced signals could be separated from possible launch induced signals.

4.2 Background Signal Analyses

Figure 4.2-1 shows the power spectrum calculated from the data obtained with the ELF0 sensor. The periodogram was obtained by segmenting the 65536 sample length record into 1024 bit segments, applying a Hanning window on each segment and then averaging the spectrum of all windows. The resulting spectrum clearly shows a set of resonances at approximately 7 to 8, 14, and 21 Hz. These values are clearly indicative of Schumann resonances in the earth-ionosphere cavity. This result implies that background noise of this type could be reduced by applying an appropriate filter to the data. If the missile launch signals lie outside the stop band filter, such signals may be enhanced. In Section 4.4.1 we provide the results of this analysis.

4.3 Cross Correlation (Time Synchronization) Analysis

In order to provide a better time tie of the data, we performed an analysis of the cross correlation between the waveforms obtained at the various sites. Note that this might appear risky since geo-potential noise at very low frequencies do not have excellent spatial coherence (site-to-site distances were on the order of a kilometer); however, we still performed this analysis using the standard cross correlation routine in the MATLAB toolbox. The cross correlation used the self normalization routine so

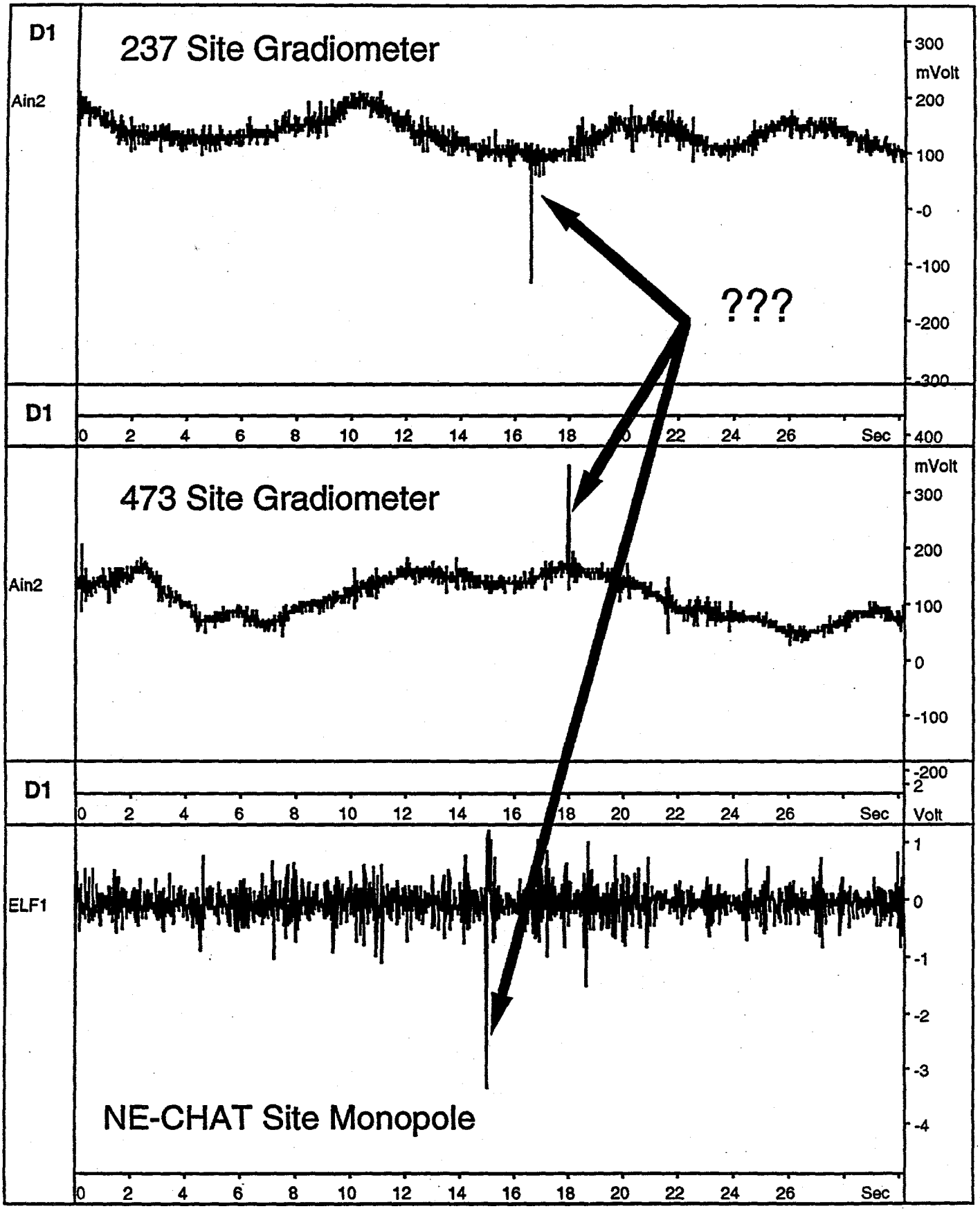

Figure 4.1-1: Simple Compaison of Three Measurement Sites. Data has been smoothed by a simple moving average in order to eliminate the 60 Hz Noise component. Also, the MLD detectors have been analyzed based on a gradiometer configuration.

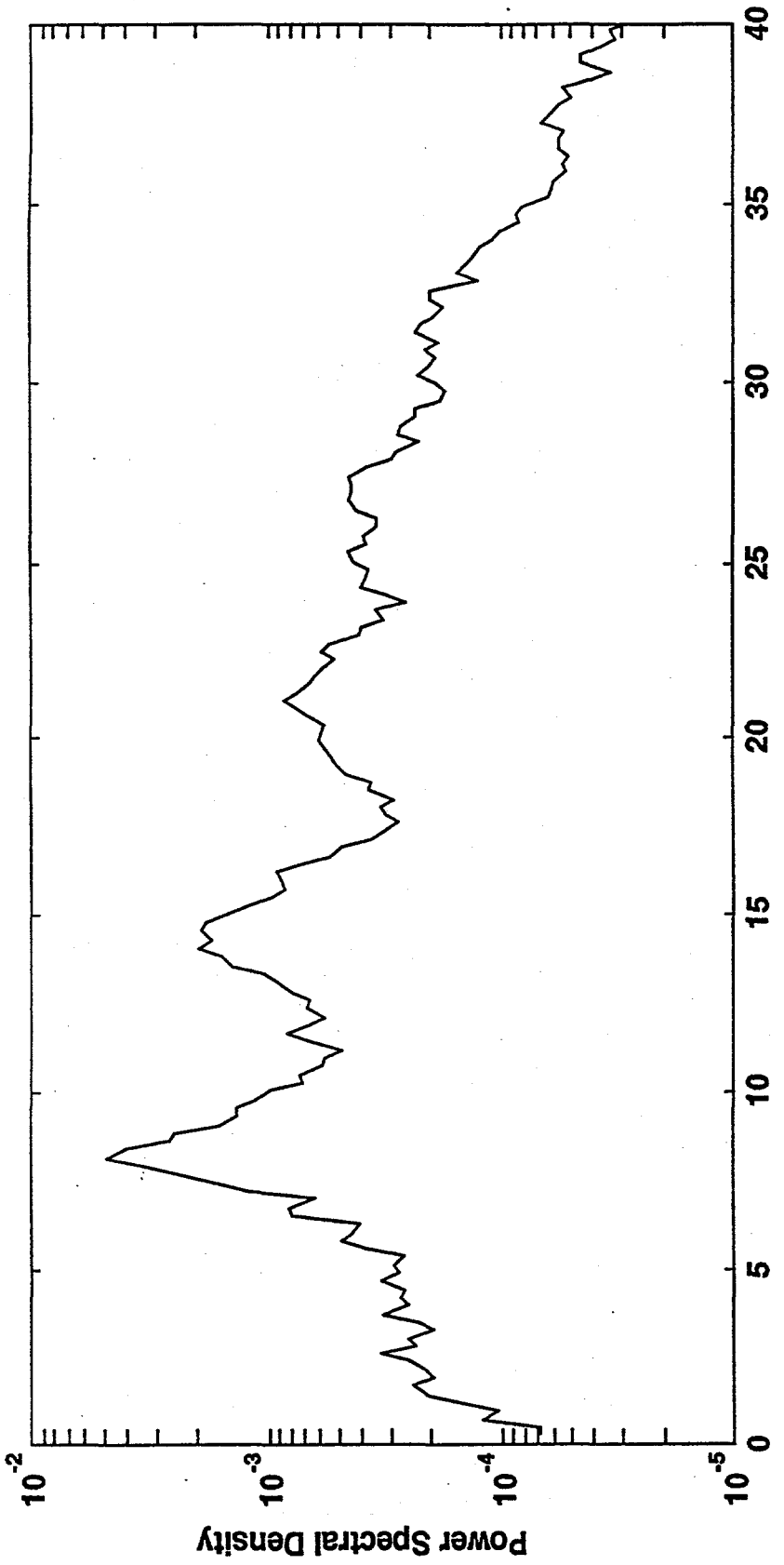

Figure 4.2-1: Power Spectrum of Data from ELF0 at CHAT Site. Spectrum shows several peaks at frequencies in the 8 to 30 Hz regime that are induced by Schumann resonances in the earth-ionosphere cavity. Lightning activity in storms around the planet lead to this behavior.

that the autocorrelation function of a given waveform would yield unity at zero offset.

Figures 4.3-1 and 4.3-2 show the results of the cross correlation of the 237 and 473 sites against the ELF0 result. All of the waveforms were numerically decimated to eliminate 60 Hz effects on the cross correlation analysis. We see that the cross correlation generates a sharply peaked distribution for both cases. Thus, there is sufficient spatial coherence to obtain an estimate of the offset time developed by our primitive time-tieing. Figures 4.3-3, 4.3-4, and 4.3-4 show the corresponding realigned waveforms for the three measurement sites. The overlap of the primary peaks in for the Chat and 473 sites are quite good. However, for the 237 site, the candidate peak (switched polarity) is embedded in heavy noise. This may be due to the power distribution site near the 237 measurement site. The 473 site was the furthest from any power distribution and the Chat site detector used added active notch filters to help reduce power line effects.

4.4 Enhanced Low Frequency Signature Evaluation

Based on the spectral analysis of the noise (presented in Section 4.2), we reexamined the data in order to see if further decimation would enhance the peak observed in the ELF0 data with respect to the other peaks that were possibly due to Schumann resonance induced noise. In Figure 4.4-1 we show the raw data that was obtained at the Chat site with ELF0. This data includes the effect of power line signals and shows a wide band of noise with numerous spikes in response. Note that the large response at early time is due to the pickup of the motion of the DAS operator while the operator moved clear of the ELF0 probe.

In Figure 4.4-2 we show the resulting waveform for the case where the data has been decimated by a factor of two. For this specific measurement, the sample rate was 240 samples per second. Thus a decimation by a factor of two will lead to a high order cutoff frequency that is just a bit below 60 Hz. This amounts to eliminating the 60 Hz and any higher order aliased harmonics from the waveform. While the heavy band of noise has been somewhat diminished, there are still numerous peaks in the data. Thus identification of a unique signature associated with the missile launch is quite difficult.

According to the noise analysis, most of the Schumann resonance effects can be eliminated by low passing the data below 8 Hz. Thus, we further decimated the ELF0 waveform by a factor of eight. Figure 4.4-3 shows the resulting waveform. Other than the early time personnel motion effects (footfall for a walking individual has a primary frequency on the order of a couple Hertz), there are only two large peaks in the data. The first one corresponds to the onset of the first missile launch. Note that there is no clear signature associated with the time of the second launch (about 30 seconds later). We do not know whether this is due to the initial plume from the first launch suppressing the second launch's signal, the initial spike being produced by some spurious control signal that controlled initial launch onset, or that the signal is just an

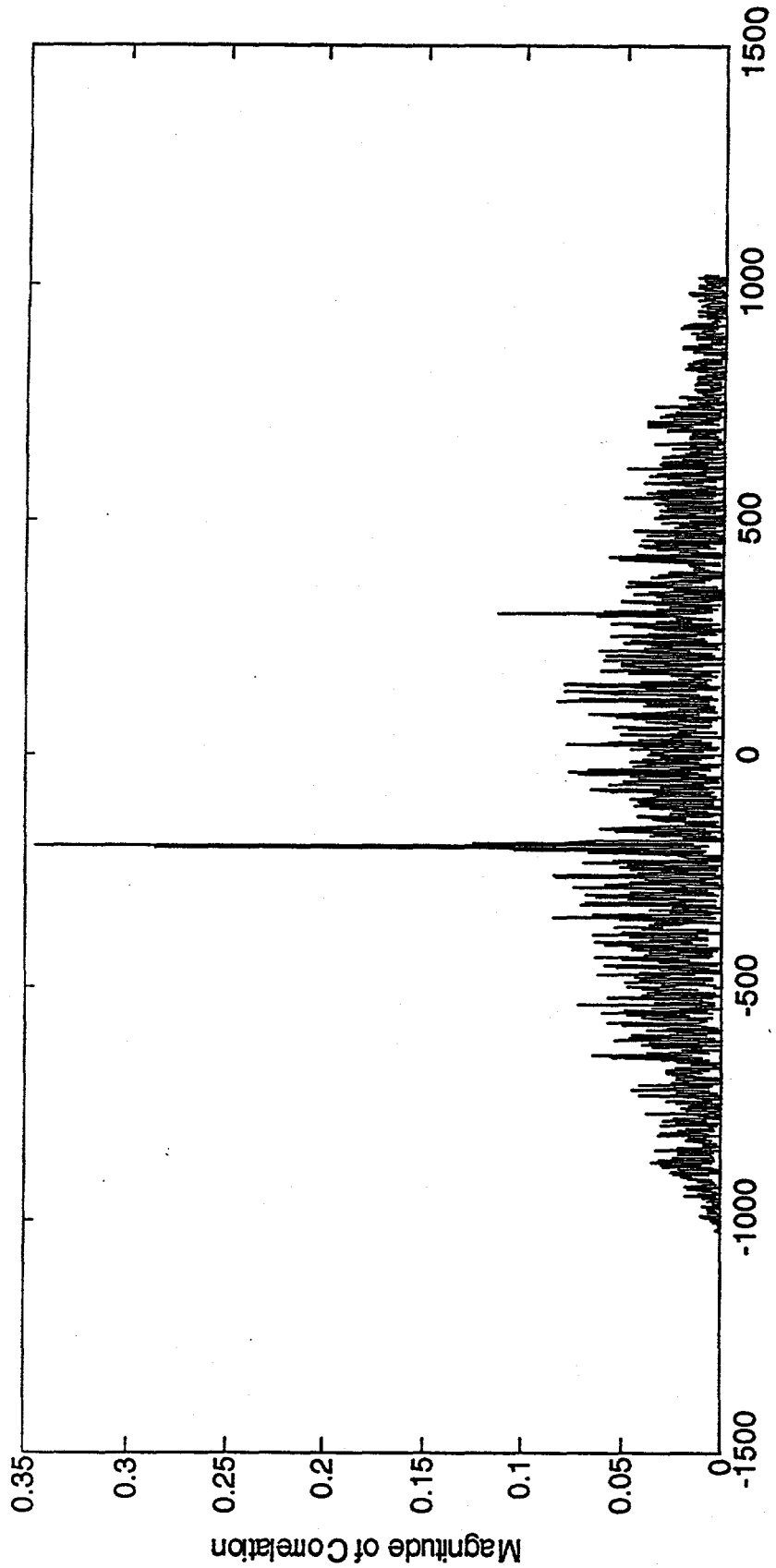

Figure 4.3-1: Result of Cross Correlation Between Chat and 473 Benchmark Sites. Result shows an offset of about 196 bins or a time difference of about 6.5 seconds between the time windows for the CHAT and 473 benchmark sites.

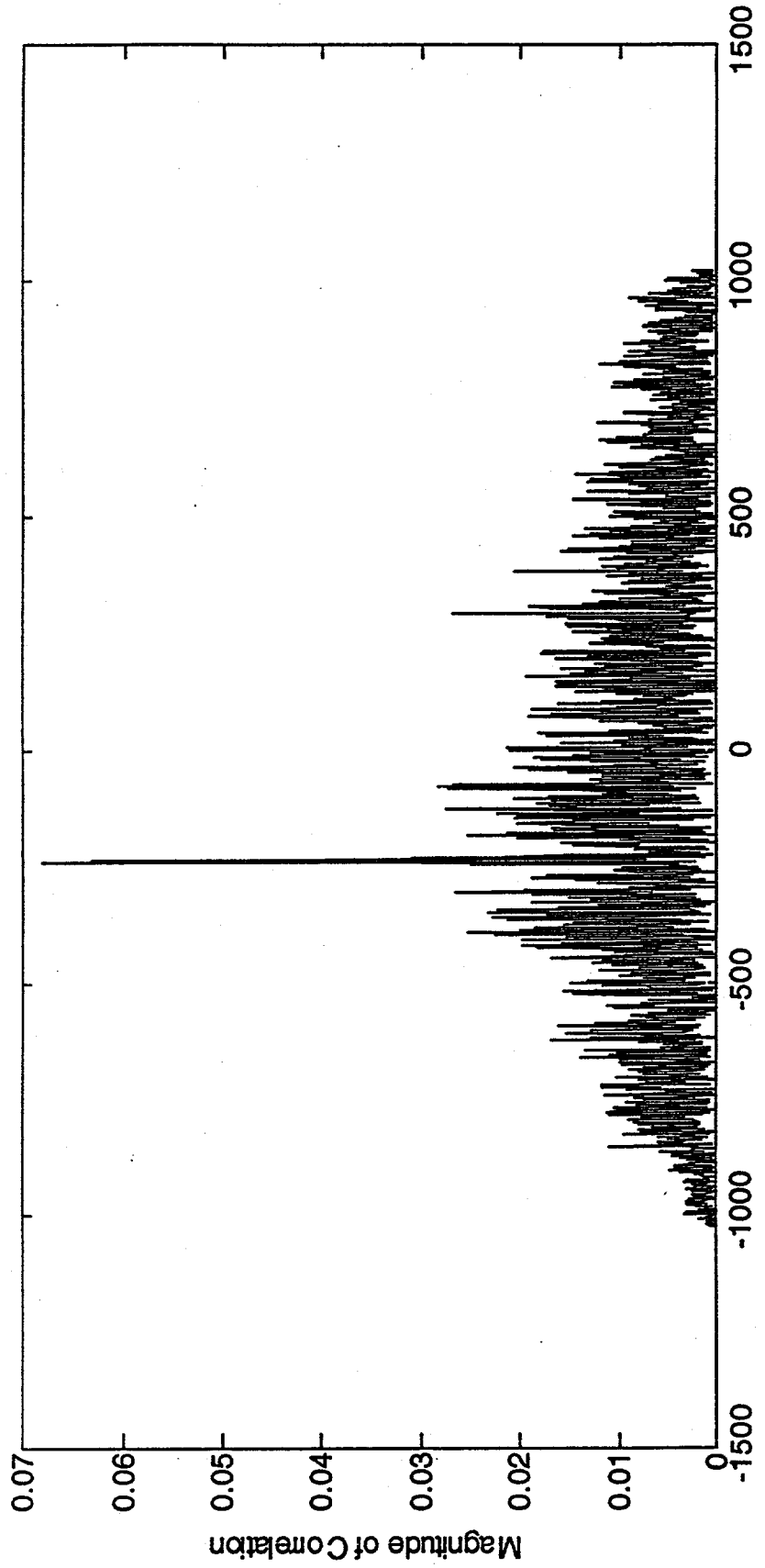

Figure 4.3-2: Result of Cross Correlation Between CHAT Site Record and End of Road 237 Site Record. Result shows an offset of the time line that corresponds to 241 bins or a time difference of about 8 seconds between the two data records.

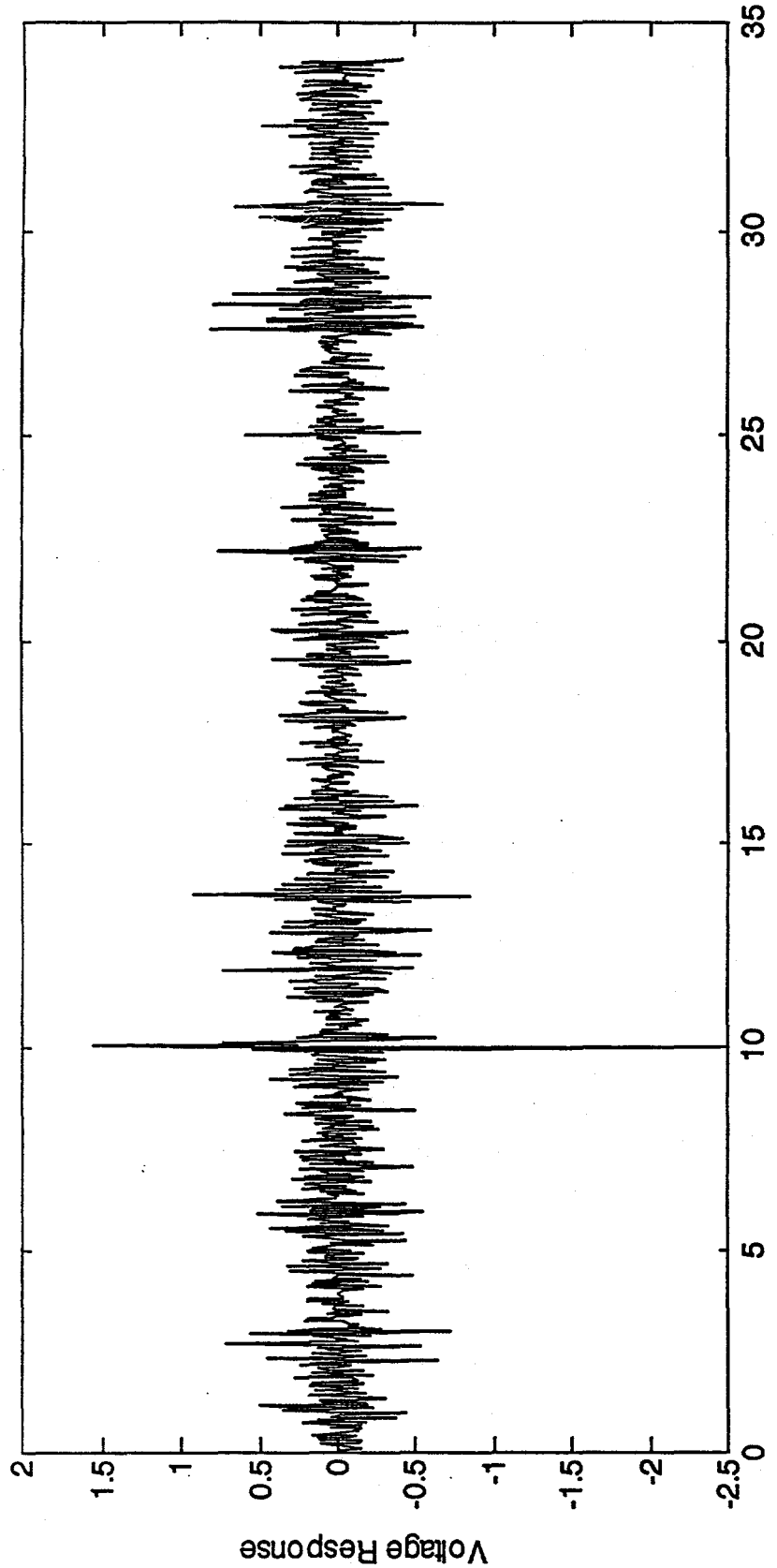

Figure 4.3-3: Baseline Time Line for ELF0 Detector. Primary peak at 10 seconds is possibly launch related. DAS operator kept running stop watch during launch and estimated launch time that coincides with the 10 second time to within 1 second.

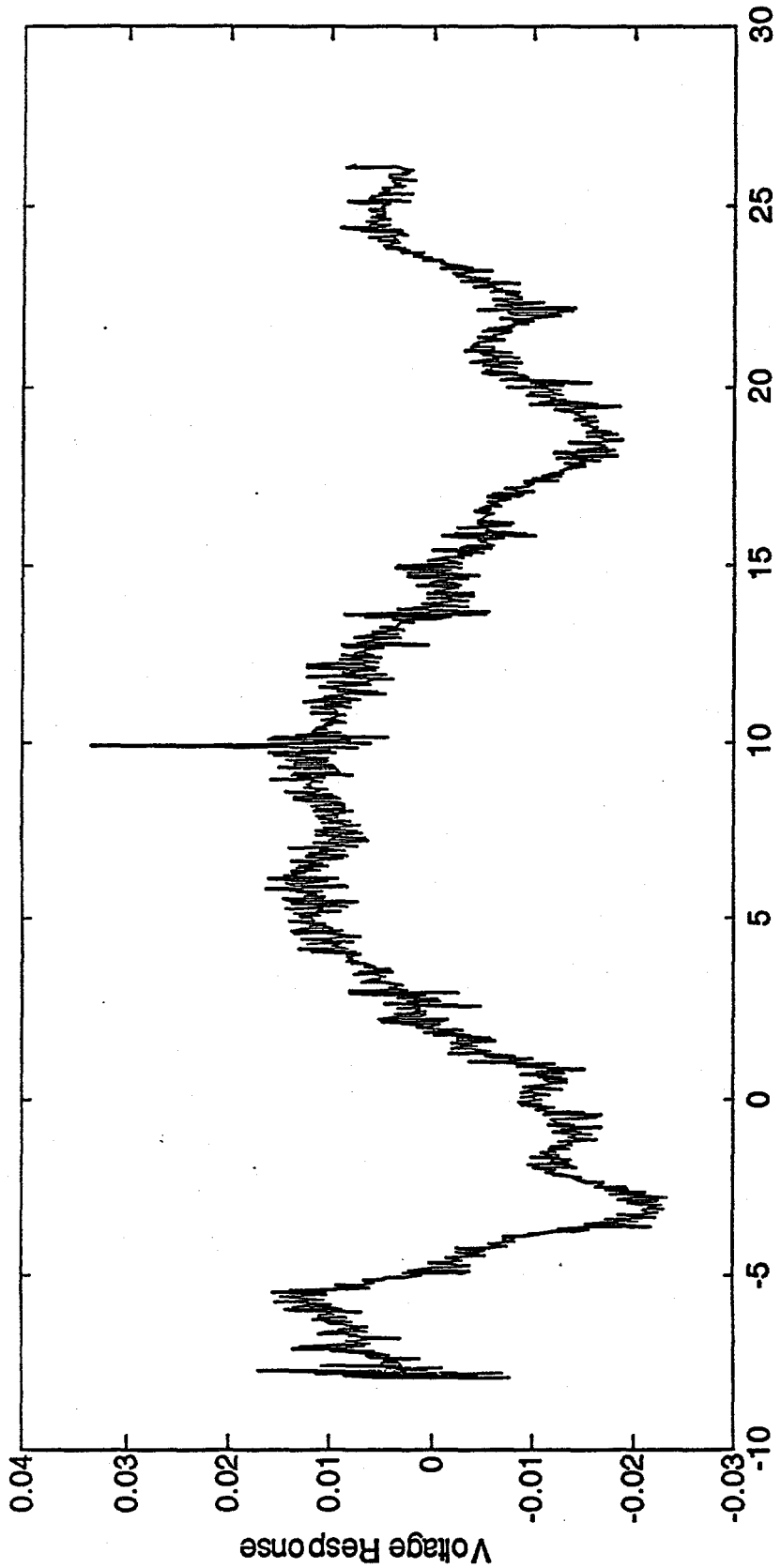

Figure 4.3-4: Shifted Waveform for 473 Benchmark Site. Waveform was shifted by time obtained through cross-correlation analysis.

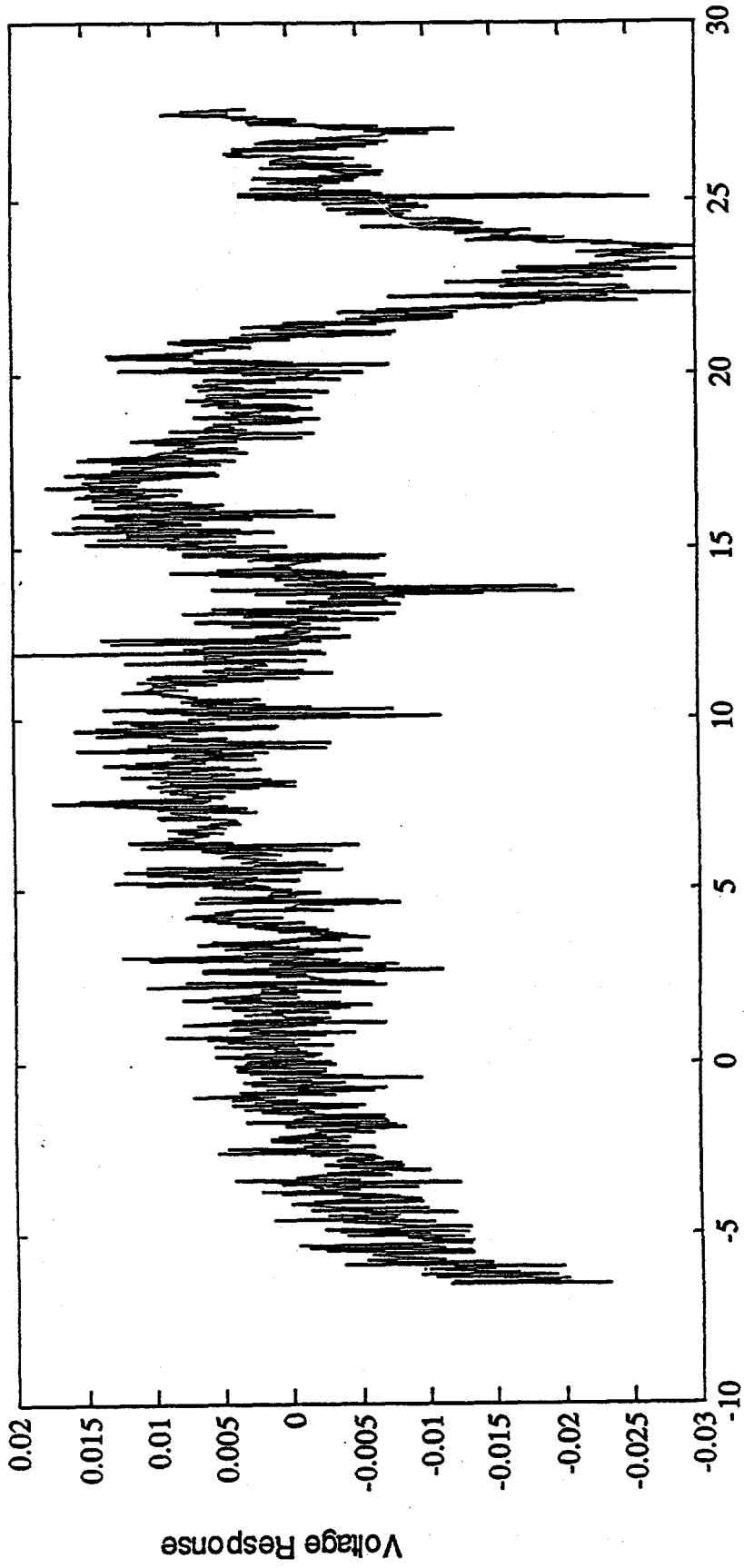

Figure 4..3-5: Shifted Waveform for End of Road 237 Site. Waveform was shifted by time obtained through cross-correlation analysis.

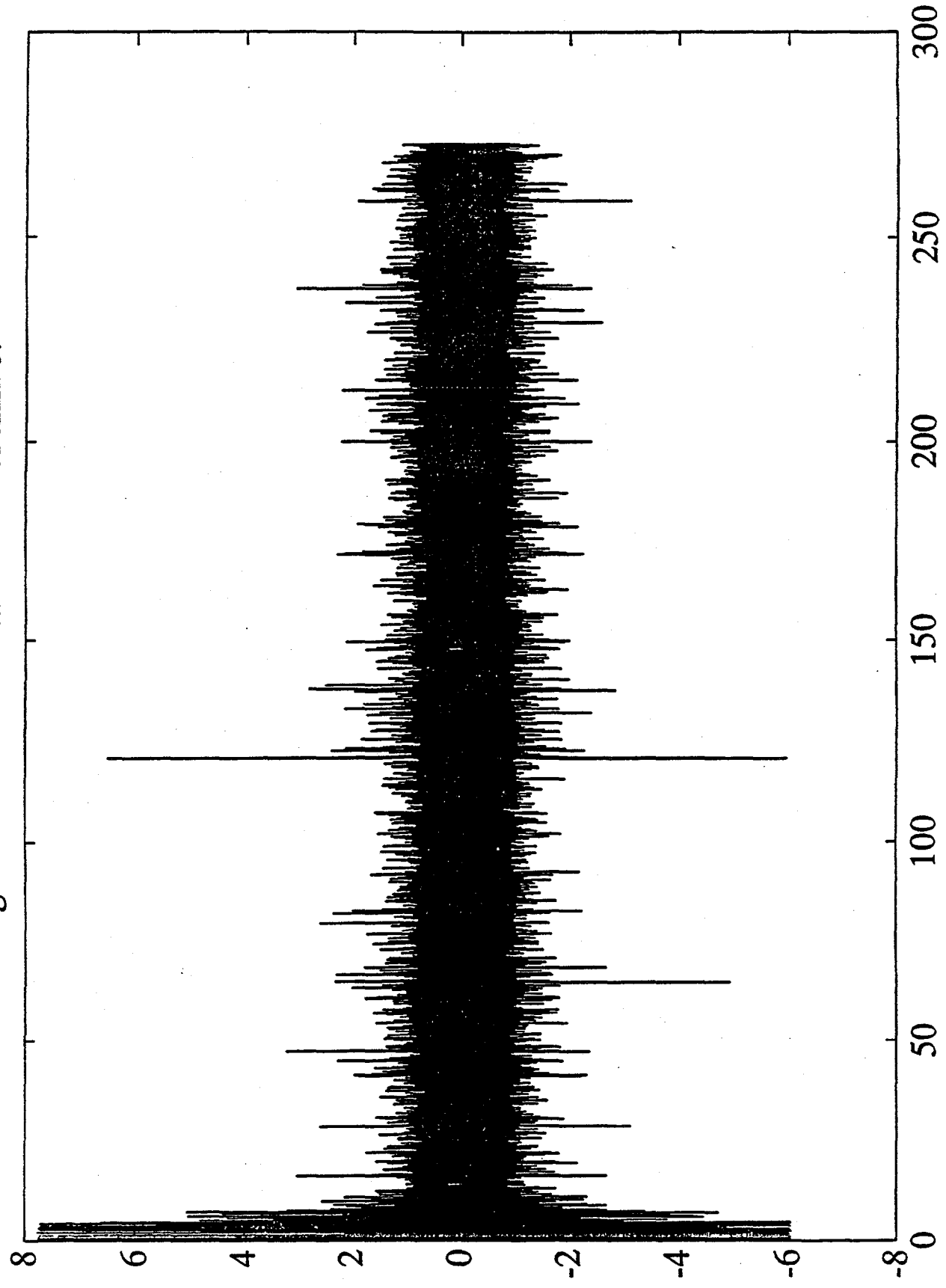

Figure 4.4-1: Full Data Record for ELF0.

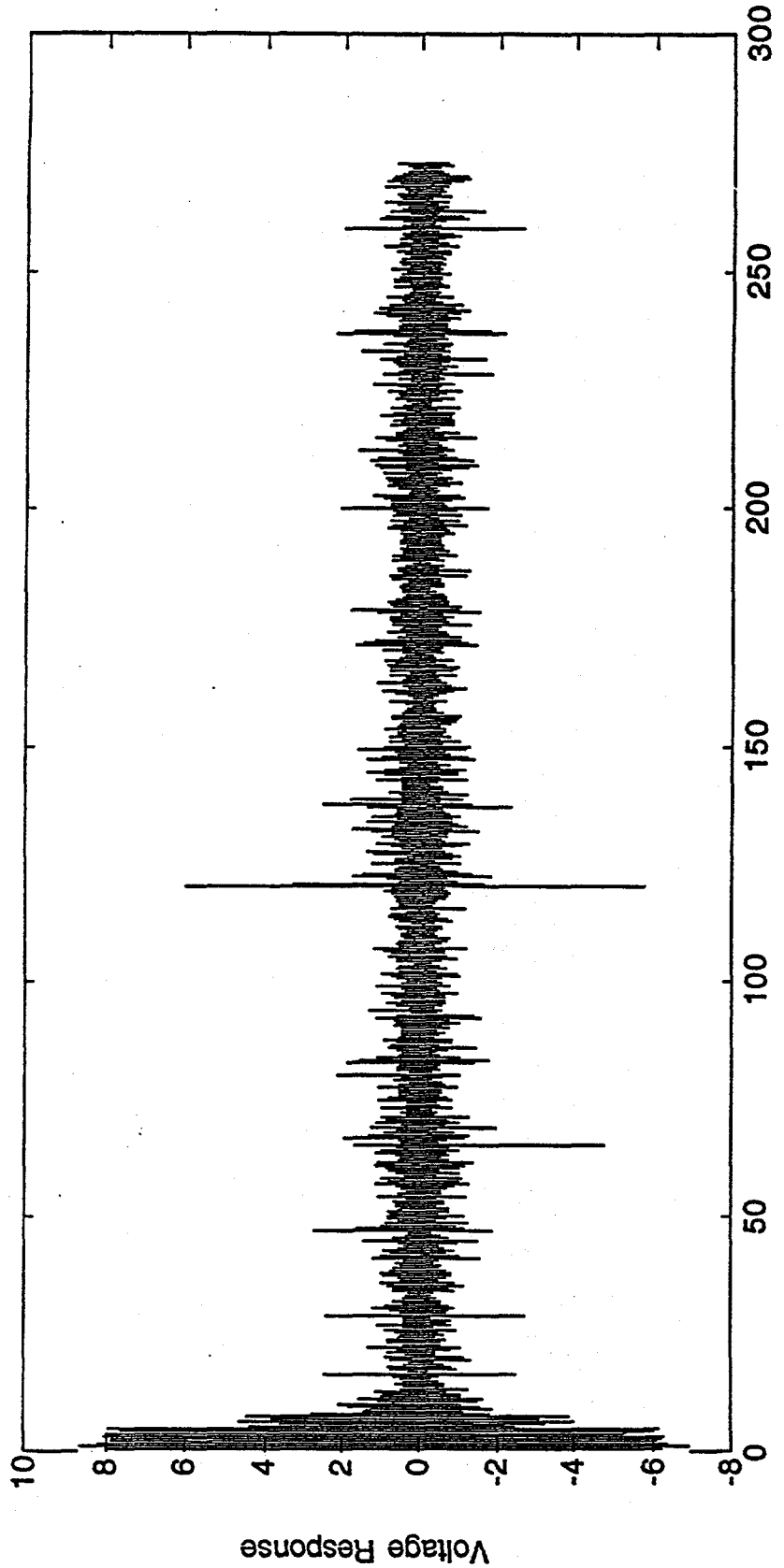

Figure 4.4-2: ELF0 Data Record Decimated by a Factor of 2.

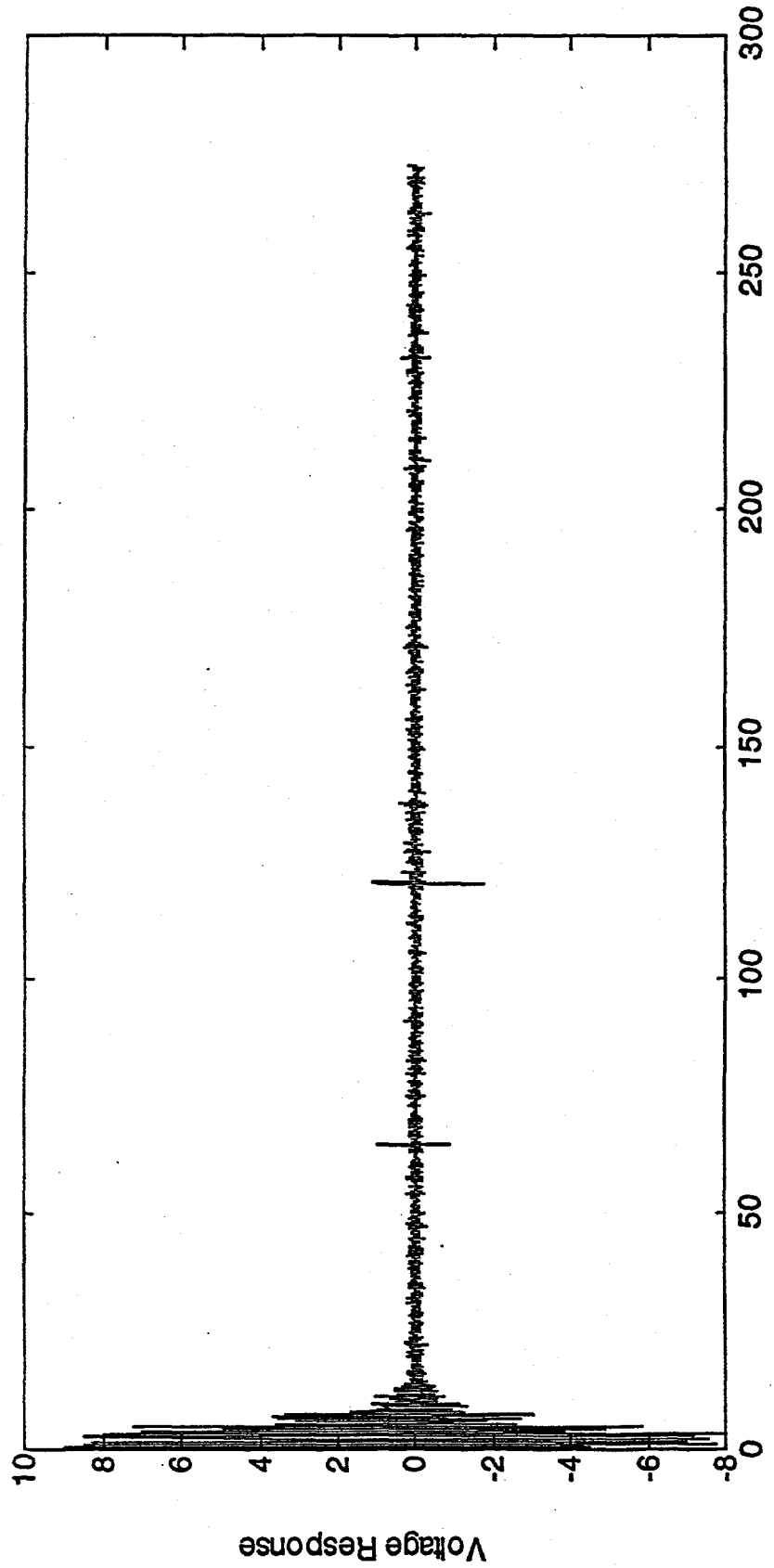

Figure 4.4-3: ELF0 Data Record Decimated by a Factor of 16.

unusual naturally induced spike that coincided with the launch time.

Additionally, there is a large spike in the decimated data at a time of about 60 seconds after launch. The raw data shows a large transient at this time that has a strong damped sine wave appearance with interference effects. Spectral transform of this impulse again shows strong Schumann-like resonances. Because the transform also shows a strong "DC" component, it is not likely that the signal was produced by a distant source which would experience dispersive smearing and a loss of the DC component. This argues for a localized source. While there was a storm off the west coast of Mexico during the launch, we do not suspect that lightning transients at such a range would lead to this type of behavior. An alternate possibility may be that at this time the missile was reaching a high enough altitude that the missile/plume may have heavily interacted with the D-layer and initiated some unusual Schumann resonance excitation.

4.5 High Frequency Signature Evaluation

As discussed above, there is the possibility that other physical processes may lead to signatures that have rather high frequency components. These components may be tied to turbulent phenomena which also result in the acoustical emission of the missile. For this reason, we extended the low pass cutoff of the MLD filters in order to look for other signatures than those that could be detected with the ELF0 detector. Accordingly, we developed some power spectrum periodograms of the 473 detector for times just prior to and directly after the initial missile launch. Figures 4.5-1 and 4.5-2 shows the resulting spectra for these two cases.

In Figure 4.5-1 (prior to launch) we see a broad band spectral response that has odd harmonics of the 60 Hz power distribution system as well as a "1/f" type noise signal at frequencies below about 400 Hz. Above 400 Hz the noise floor flattens out into a flat region that is possibly indicative of the dynamic range of the digitized data. Note that the sampling rate for the experimental runs was selected to ensure that and additional power line harmonics beyond 900 Hz would be folded back down on one of the 60 Hz harmonics. Thus, we see that there is no apparent aliased peaks from high frequency sources that might exist above 900 Hz.

In contrast to this result, Figure 4.5-2 shows the resulting spectrum for the time period just after launch. This spectrum shows a number of high frequency peaks that are not present in data prior to launch. At this time we do not know whether or not his is a missile/plume induced effect or may be due to other operations signals in the WSMR area. It would be interesting to obtain data on the acoustical output of the Lance system to see if there is any correlation with the MLD spectrum. Of course with the restricted amount of data obtained during this test it is at present difficult to determine whether 1) this signal is due to turbulent effects cross coupling to an electromagnetic effect, 2) this signal is just a microphonic pickup of the acoustical output of the missile, or 3) is induced by some other source at WSMR.

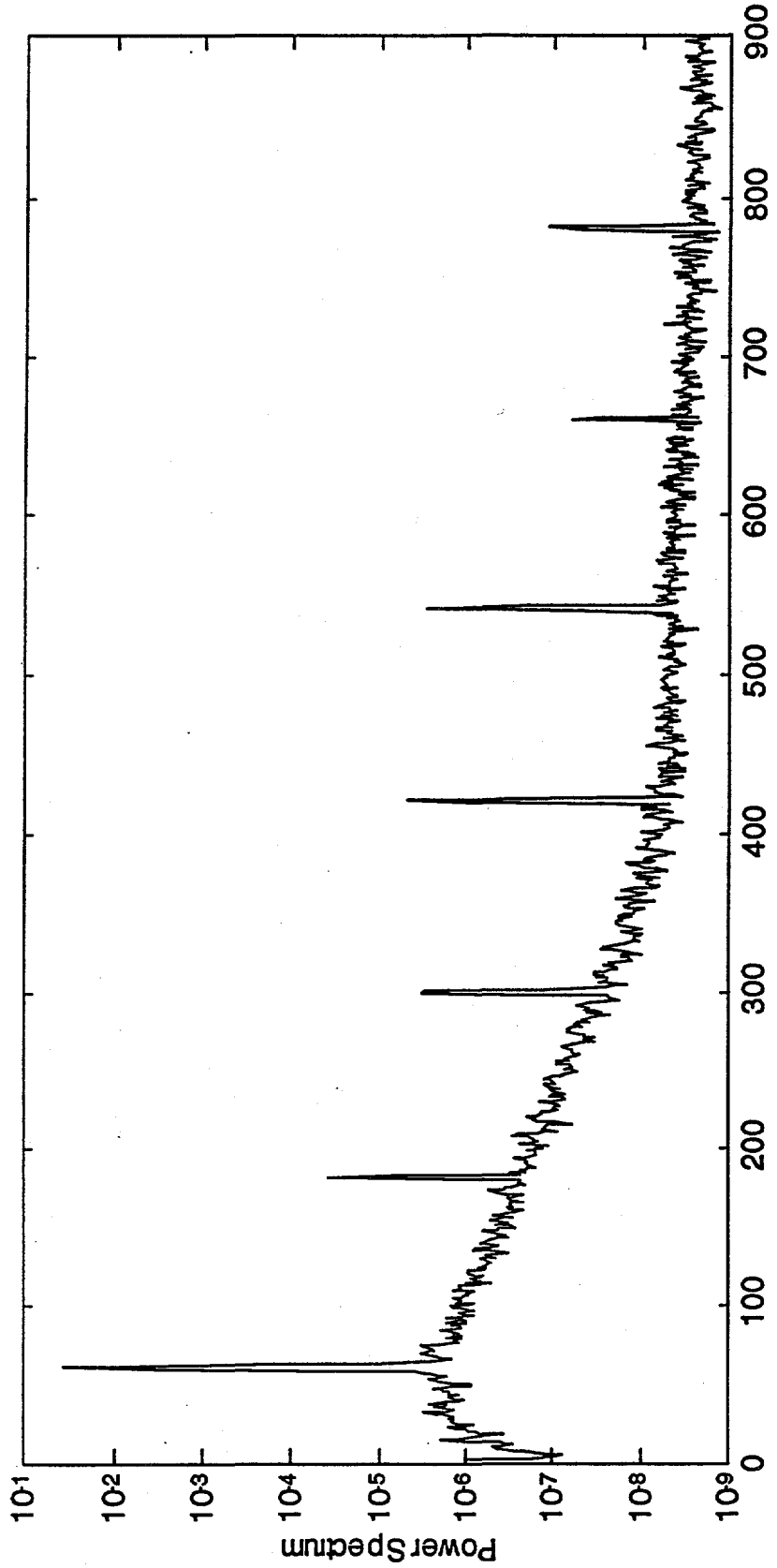

Figure 4.5-1: Power Spectum Prior to Launch for Site at End of Road 237. Narrow peaks correspond to harmonics of power line. Sampling rate (555.532 µs per sample) selected to ensure wrapping of higher aliased power line harmonics back onto lower frequency harmonics.

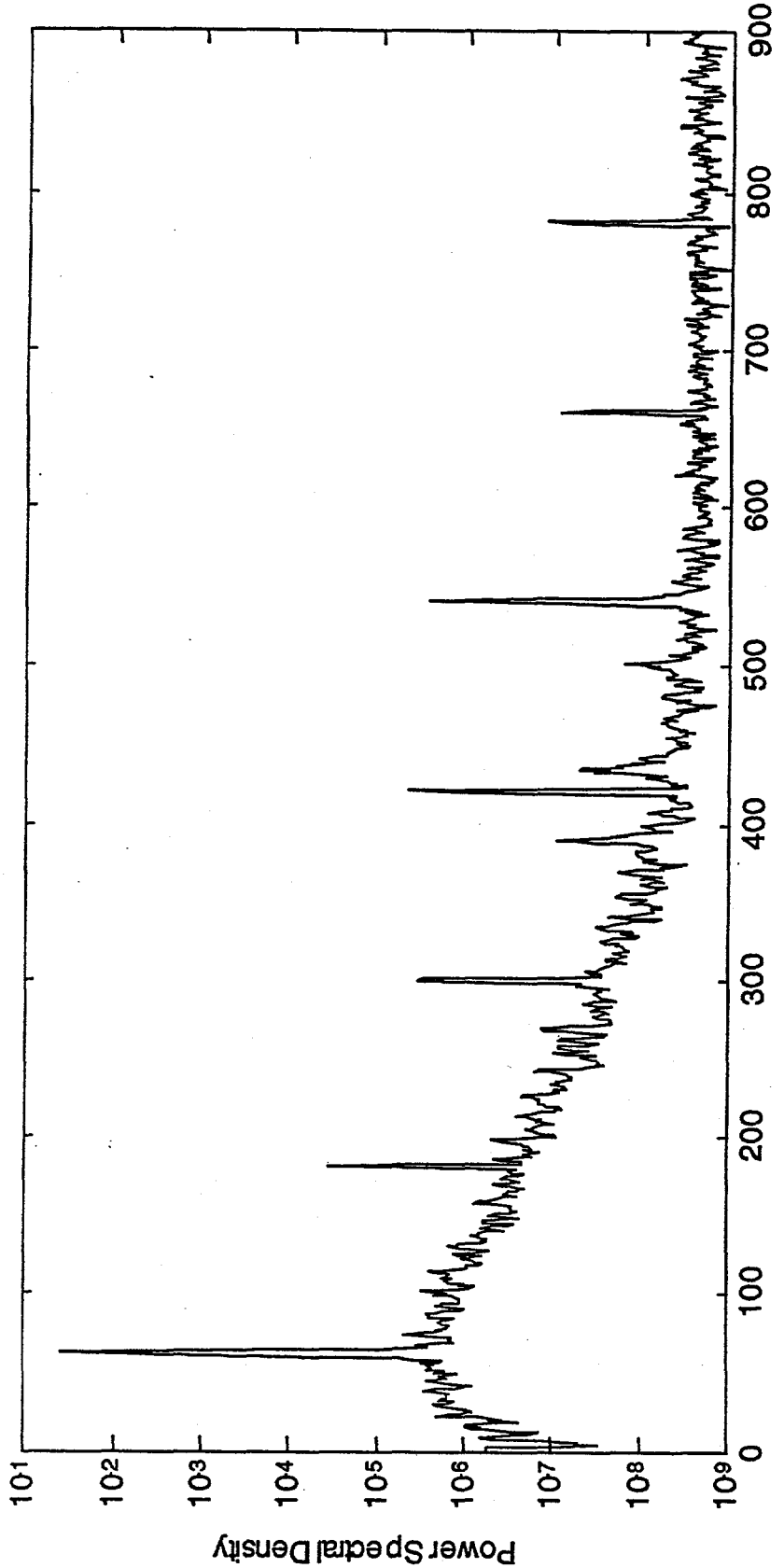

Figure 4.5-2: Power Spectum after Launch for Site at End of Road 237. Primary narrow peaks correspond to harmonics of power line. Sampling rate (555.532 µs per sample) selected to ensure wrapping of higher aliased power line harmonics back onto lower frequency harmonics. Spectrum also shows additional peakds at 390, 430, and 500 Hz that did not appear in power spectrum of data measured just prior to launch.

5.0 Summary

Initial off line examination of the data failed to locate strong event dependent information for all but one of the detectors. Primary factors contributing to the apparent low missile detection signature was natural and manmade noise sources as well as less than optimal instrumentation calibration and checkout. Additional off-line analysis and application of signal processing tools allowed us to identify a definite event dependent signature.

The few km range to the missile launch site, combined with extensive 60Hz background signals, buried the detection signal in the noise. This required us to implement more sophisticated signal processing tools (used to eliminate the 60 Hz and earth-ionosphere cavity resonance effects) to find the missile signature. Other advanced signal processing tools (such as those proposed for our upcoming DARPA Phase II program) may allow the extraction of specific categories of signals at even lower S/N ratios. These new signal processing algorithms are easily built into the on-line instrumentation and recording computers, allowing real-time extraction and identification of the event.

Additional examination of the data also showed a problem with the gradiometer configuration deployed at two of the measurement sites. These gradiometers were based on new, unproven wide bandwidth detectors with LLNL supplied Data Acquisition Tape recorders used for monitoring signal output. The time waveforms from these detectors showed strong contamination with frequencies below a few Hertz which greatly reduced dynamic range and correlation capabilities. This effect may be due to a grounding problem or some interaction between the sensors and the data acquisition system. Improved sensors/instrumentation with full end-to-end calibration across the spectrum of operation would help resolve problems that may be associated with the equipment used for this test.